Fig. 2. This patient (case 7) had complete atelectasis of the left whole lung. Bronchoscopy shows a polypoid lesion, which almost completely occluded the left main bronchus (A). Chest CT on the coronal view shows a well-circumscribed enhanced mass with occlusion of left main bronchus (B).

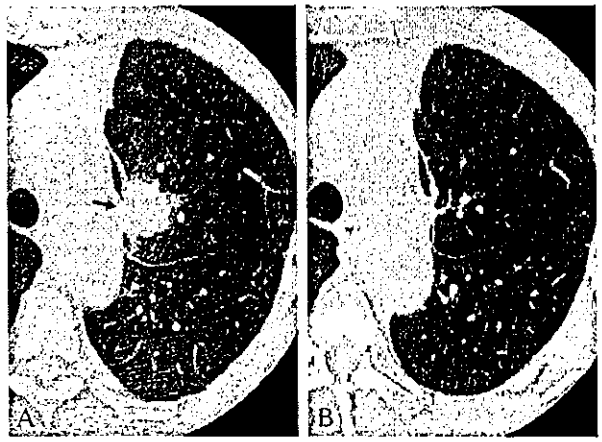

Fig. 3. On the CT findings, one patient (case 6) suffered from margin relapse, which developed adjacent to resected staple line (arrow), 4 years after initial resection (A). About 8 months later, spontaneous resolution of the tumor has been observed (B).

the definitive diagnosis because they followed a variety of lesions such as inflammation or malignancy. One patient (case 6) had an erroneous diagnosis of adenocarcinoma by aspiration cytology, because the cytologic findings showed atypical epithelial-like cells with lymphocytes and histiocytes. For all these patients, the diagnostic procedure was surgical excision. Although an intraoperative frozen section was done for the tumor in all cases, the confirmed diagnosis could not be made. However, all the tumors were regarded as low-grade malignancy because of low nuclear atypia and infrequent mitosis. The extent of surgical excision was as follows: segmentectomy in four patients, segmental bronchial resection in one, lobectomy in two, bilobectomy with bronchoplasty in one, and extirpation in one. Complete resection of the tumor was accomplished in eight patients (89%). One patient (case 7) had a pathological residual tumor in the submucosal tissue of the left main bronchus. None of the operations resulted in death. On the follow-up CT one patient (case 6) had a suspected recurrent tumor developing adjacent to the resected line four years after the initial resection, although this tumor was not evaluated histologically. Interestingly, spontaneous resolution of this tumor has been observed (Fig. 3). In the other eight patients, no recurrence of IMT occurred. All of the patients have remained healthy.

3.2. Pathological and ultrastructural findings

The resected tumor size ranged from 1.0 to 4.0 cm in the greatest diameter, with a mean of 2.8 cm. For gross appearance, most of the tumors were well-circumscribed masses without fibrous capsules and yellow to whitish in color on cut section.

Microscopically, the lesions consisted of a variety of inflammatory and mesenchymal cells, including plasma cells, histiocytes, lymphocytes, and spindle cells. All of the tumors showed interlacing fascicles, or a storiform pattern of spindle cells and an admixture of diverse inflammatory cells (Fig. 4A). The spindle cells had low cellular atypia and no mitotic activity (Fig. 4B). Blood vessel invasion was identified in one instance (case 4).

Immunohistochemically, most of spindle cells in all nine cases showed diffuse and strong reactivity for vimentin. All tumors exhibited reactivity for smooth muscle actin (Fig. 5). The staining was diffuse in eight of nine cases (89%) and focal in one (11%). One tumor exhibited focal staining for desmin. All tumors were negative for cytokeratins, CD34, S100 protein, and epithelial membrane antigen.

Ultrastructurally, two tumors (cases 3 and 9) out of four contained a varying proportion of myofibroblastic cells, as well as fibroblastic cells with a prominent Golgi apparatus

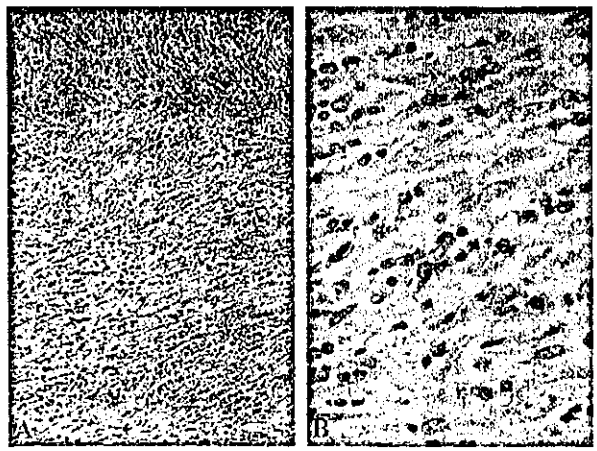

Fig. 4. Photomicrographs show an inflammatory myofibroblastic tumor. The lesion is composed of spindle cells arranged in interlacing fascicles, with admixed diverse inflammatory cells (A). The spindle cells have low cellular atypia and no mitotic activity, and the inflammatory cells are mature (B). (both, hematoxylin-eosin; A, original magnification 100 ×, B, original magnification 400 ×).

Fig. 5. Immunohistochemically, the spindle cells of the lesion show diffuse and strong reactivity for smooth muscle actin (immunohistochemistry for smooth muscle actin, original magnification 200 ×).

and well developed rough endoplasmic reticulum (RER). The myofibroblastic tumor cells were recognized by the presence of an often well developed branching RER and primarily peripheral bundles of actin microfilaments with interspersed fusiform densities (Fig. 6). Subplasmalemmal attachment plaques, focal basal lamina-like material, and micropinocytotic vesicles were present to variable degrees in these cells. The other tumors consisted of fibroblastic and histiocytic cells with lysosomes and lipid droplets.

4. Discussion

IMT of the lung is rare, and its incidence is reported to be 0.04–1% of all tumors of the lung [1,3]. Although IMT can grow at a wide variety of other sites [19,20], it usually arises within the lung [1]. Concerning the age of patients at diagnosis, the mean age of 44.6 years in this study was relatively older than those reported previously [4,5,7,10,17]. According to previous reports, most of the patients were under 40 years old, with a mean age of 27–50 years. There was no predominance of either sex. The precise etiology of IMT of the lung is still unknown. Although a history of prior pulmonary infection in some patients with IMT has been pointed out [4], this type of patient was not found in the present study. Patients with IMT usually are asymptomatic, with a solitary nodule or mass detected by routine chest roentgenogram [5]. Endobronchial growth of IMT has only rarely been observed [2,6,7], with a prevalence of between 0 and 12%. In this study we had a relatively high prevalence (two of nine, or 22%) of patients with endobronchial growth of IMT. On the other hand, it has been known that IMT carries a risk of extension to neighboring organs [1,4,9,11], in particular to the mediastinum, although we did not observe this. Preoperative laboratory findings indicated that only one patient (11%) with a solitary pulmonary mass had an elevated CRP rate and WBC count, and the IMT appeared to have no connection with these laboratory findings [3,4]. The preoperative diagnosis of IMT is seldom confirmed, and small biopsied specimens are generally considered insufficient for diagnosis because of the predominance of inflammatory cells.

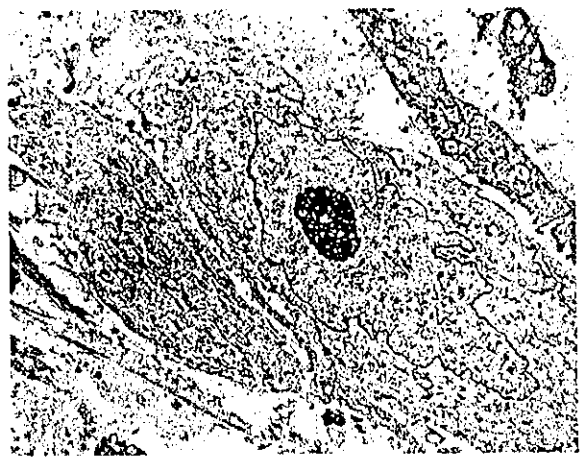

Fig. 6. Ultrastructurally, the myofibroblastic tumor cell is recognized by the presence of a well developed branching RER and primarily peripheral bundles of actin microfilaments with interspersed fusiform densities.

Pathologically, IMT is composed of a variable inflammatory and mesenchymal cellular mixture including plasma cells, histiocytes, lymphocytes, and spindle cells. Therefore, depending on the predominant cellular components, many synonyms for this disease have been described. In 1990, Pettinato and colleagues referred to this entity as IMT because the bulk of the lesion invariably consisted of not specific inflammatory cells, but proliferative myofibroblasts and fibroblasts [17]. Most of the spindle cells were myofibroblasts, which showed immunohistochemical staining for vimentin and smooth muscle actin, and consistent ultrastructural features. The spindle cells commonly have low cellular atypia and no mitotic activity. Inflammatory cells are mature and have no cellular atypia, and do not show monoclonal proliferation [3,17,18]. IMT occasionally invades bronchi or blood vessels [8,18]. We treated one patient (11%) with IMT who showed blood vessel invasion (case 4). However, it is doubtful that these are truly the tumor infiltrations, because the existing histologic architecture of the lung can also be destroyed by infiltration of only inflammatory cells. Furthermore, distant metastases from IMT are hardly ever reported. The differential diagnosis of IMT is multifarious because of its variable cellular admixture. It includes malignant lymphoma, lymphoid hyperplasia, pseudolymphoma, plasmacytoma, malignant fibrous histiocytoma, sarcomatoid carcinoma of the lung, sclerosing hemangioma, sarcoma, and/or nodular chronic pneumonitis. These lesions can be differentiated by careful attention to cellular atypia, necrosis, mitotic activity, immunoreactivity, or clonality [1,9,18]. IMT of the lung also has the histologic resemblance to the fibromas of the parietal or visceral pleuras. The fibromas shows short fascicles or haphazard fashion of spindle cells with few inflammatory cells, whereas IMT shows interlacing

fascicles or a storiform pattern of spindle cells and an admixture of diverse inflammatory cells [21].

Although the notion of IMT being a reactive lesion or a neoplasm had been controversial, IMT has been recently thought of as a neoplasm rather than a reactive lesion because of clonal chromosomal abnormalities [15], chromosomal rearrangements involving the ALK receptor tyrosine-kinase locus region (chromosome band 2p23) [16], or DNA aneuploidy in IMT [14]. IMT usually grows locally and slowly. Therefore, taking into account these histopathologic and biological findings, IMT may be regarded as low-grade malignancy or benign tumor.

Surgical resection is recommended as the treatment of choice. Cerfolio and colleagues reported that the residual tumor became enlarged in 60% of patients who had incomplete resection [1]. They advocated the importance of initial complete resection of the tumor. Surgical removal usually fills the role of both diagnosis and treatment. The effectiveness of radiotherapy, chemotherapy, or steroids is uncertain [1,12]. The spontaneous regression of IMT has been reported only infrequently [9]. Likewise, we cared for one patient with spontaneous regression of the recurrent tumor, although this was not confirmed histologically. The causes of these remissions are unknown. The outcome after resection is usually excellent, and all of the patients in this study have also remained well over the longer term. However, long-term follow-up is necessary because of reported cases of recurrences many years after resection [2,22].

In conclusion, IMT of the lung is rare. Histopathologically, IMT is characterized by myofibroblasts that are mixed with chronic inflammatory components, consisting of plasma cells, lymphocytes, and histiocytes. Surgical resection, when possible, is recommended as the treatment of choice. The outcome after complete resection is excellent.

References

[1] Cerfolio RJ, Allen MS, Nascimento AG, Deschamps C, Trastek VF, Miller DL, Pairolero PC. Inflammatory pseudotumors of the lung. Ann Thorac Surg 1999;67:933–6.

[2] Matsubara O, Tan-Liu NS, Kenney RM, Mark EJ. Inflammatory pseudotumors of the lung: progression from organizing pneumonia to fibrous histiocytoma or to plasma cell granuloma in 32 cases. Hum Pathol 1988;19:807–14.

[3] Ishida T, Oka T, Nishino T, Tateishi M, Mitsudomi T, Sugimachi K. Inflammatory pseudotumor of the lung in adults: radiographic and clinicopathological analysis. Ann Thorac Surg 1989;48:90–5.

[4] Berardi RS, Lee SS, Chen HP, Stines GJ. Inflammatory pseudotumors of the lung. Surg Gynecol Obstet 1983;156:89–96.

[5] Agrons GA, Rosado-de-Christenson ML, Kirejczyk WM, Conran RM, Stocker JT. Pulmonary inflammatory pseudotumor: radiologic features. Radiology 1998;206:511–8.

[6] Calderazzo M, Gallelli A, Barbieri V, Roccia F, Pelaia G, Tranfa CME, Cavaliere S, Zorzi F. Inflammatory pseudotumour of the lung presenting as an airway obstructive syndrome. Respir Med 1997;91: 381–4.

[7] Bahadori M, Liebow AA. Plasma cell granulomas of the lung. Cancer 1973;31:191–208.

[8] Warter A, Satge D, Roeslin N. Angioinvasive plasma cell granulomas of the lung. Cancer 1987;59:435–43.

[9] Mandelbaum I, Brashear RE, Hull MT. Surgical treatment and course of pulmonary pseudotumor (plasma cell granuloma). J Thorac Cardiovasc Surg 1981;82:77–82.

[10] Copin MC, Gosselin BH, Ribet ME. Plasma cell granuloma of the lung: difficulties in diagnosis and prognosis. Ann Thorac Surg 1996; 61:1477–82.

[11] Urschel JD, Horan TA, Unruh HW. Plasma cell granuloma of the lung. J Thorac Cardiovasc Surg 1992;104:870–5.

[12] Imperato JP, Folkman J, Sagerman RH, Cassady JR. Treatment of plasma cell granuloma of the lung with radiation therapy: a report two cases and a review of the literature. Cancer 1986;57:2127–9.

[13] Grossman RE, Bemis EL, Pemberton AH, Narodick BG. Fibrous histiocytoma or xanthoma of the lung with bronchial involvement. J Thorac Cardiovasc Surg 1973;65:653–7.

[14] Biselli R, Ferlini C, Fattorossi A, Boldrini R, Bosman C. Inflammatory myofibroblastic tumor (inflammatory pseudotumor): DNA flow cytometric analysis of nine pediatric cases. Cancer 1996; 77:778–84.

[15] Snyder CS, DellAquila M, Haghighi P, Baergen RN, Suh YK, Yi ES. Clonal changes in inflammatory pseudotumor of the lung: a case report. Cancer 1995;76:1545–9.

[16] Lawrence B, Perez-Atayde A, Hibbard MK, Rubin BP, Cin PD, Pinkus JL, Pinkus GS, Xiao S, Yi ES, Fletcher CD, Fletcher JA. TPM3-ALK and TPM4-ALK oncogenes in inflammatory myofibroblastic tumors. Am J Pathol 2000;157:377–84.

[17] Pettinato G, Manivel JC, De Rose N, Dehner LP. Inflammatory myofibroblastic tumor (plasma cell granuloma): clinicopathologic study of 20 cases with immunohistochemical and ultrastructural observations. Am J Clin Pathol 1990;94:538–46.

[18] Matsubara O, Mark EJ, Ritter JH. Pseudoneoplastic lesions of the lungs, pleural surfaces, and mediastinum. In: Wick MR, Humphrey PA, Ritter JH, editors. Pathology of pseudoneoplastic lesions. New York: Lippincott-Raven, Inc.; 1997. p. 100–9.

[19] Perrone T, De Wolf-Peeters C, Frizzera G. Inflammatory pseudotumor of lymph nodes: a distinctive pattern of nodal reaction. Am J Surg Pathol 1988;12:351–61.

[20] Anthony PP, Telesinghe PU. Inflammatory pseudotumor of the liver. J Clin Pathol 1986;39:761–8.

[21] Colby TV, Koss MN, Travis WD. Fibrous and fibrohistiocytic tumors and tumor-like conditions. In: Rosai J, Sobin LH, editors. Atlas of tumor pathology. 3rd series. Tumors of the lower respiratory tract, vol. 13. Washington: Armed Forces Institute of Pathology (AFIP); 1995. p. 203–34.

[22] Weinberg PB, Bromberg PA, Askin FB. Recurrence of a plasma cell granuloma 11 years after initial resection. South Med J 1987;80: 519–21.

Prognostic Significance of MRI Findings in Patients with Myxoid–Round Cell Liposarcoma

Ukihide Tateishi[1]
Tadashi Hasegawa[2]
Yasuo Beppu[3]
Akira Kawai[3]
Mitsuo Satake[1]
Noriyuki Moriyama[1]

OBJECTIVE. The aims of this study were to determine the prognostic significance of MRI findings in patients with myxoid–round cell liposarcomas and to clarify which MRI features best indicate tumors with adverse clinical behavior.

MATERIALS AND METHODS. The initial MRI studies of 36 pathologically confirmed myxoid–round cell liposarcomas were retrospectively reviewed, and observations from this review were correlated with the histopathologic features. MR images were evaluated by two radiologists with agreement by consensus, and both univariate and multivariate analyses were conducted to evaluate survival with a median clinical follow-up of 33 months (range, 9–276 months).

RESULTS. Statistically significant MRI findings that favored a diagnosis of intermediate- or high-grade tumor were large tumor size (> 10 cm), deeply situated tumor, tumor possessing irregular contours, absence of lobulation, absence of thin septa, presence of thick septa, absence of tumor capsule, high-intensity signal pattern, pronounced enhancement, and globular or nodular enhancement. Of these MRI findings, thin septa ($p < 0.05$), a tumor capsule ($p < 0.01$), and pronounced enhancement ($p < 0.01$) were associated significantly, according to univariate analysis, with overall survival. Multivariate analysis indicated that pronounced enhancement was associated significantly with overall survival ($p < 0.05$).

CONCLUSION. Contrast-enhanced MRI findings can indicate a good or adverse prognosis in patients with myxoid–round cell liposarcomas.

Liposarcomas are classified into well-differentiated, myxoid, round cell, and pleomorphic subtypes. Myxoid liposarcomas are the most common subtype of liposarcoma, occurring in the extremities of adults. They are considered low-grade sarcomas with a low risk of metastasis and are associated with prolonged survival [1–5]. On the other hand, round cell liposarcomas are considered high-grade sarcomas with a higher likelihood of metastasis and mortality due to disease [1–5]. Recent studies reveal that myxoid and round cell liposarcomas belong to a continuous histopathologic spectrum characterized by a chromosome translocation t(12;16)(q13;p11) resulting in the fusion transcript of the *TLS* and *CHOP* genes [6–9]. However, diagnosis and prognostic predictions can often be complicated by lesions that contain admixed morphologic components of myxoid and round cell subtypes.

The characteristic MRI features of myxoid–round cell liposarcomas are attributable to the predominantly myxoid matrix of the tumor. Tumors appear on T2-weighted MR images as encapsulated tumors with signals that are hyperintense compared with the surrounding structures [10–14]. On contrast-enhanced studies, they often show marked or heterogeneous enhancement with nonenhanced areas corresponding to myxoid material [13, 14]. As expected from the fact that the histopathologic spectrum from myxoid to round cell liposarcomas is continuous, these tumors show considerable diversity on imaging. Therefore, it is important to review the reliability of MRI features for characterizing myxoid–round cell liposarcomas. The objectives of this study were to determine the prognostic significance of MRI findings in patients with myxoid–round cell liposarcomas and to clarify which MRI features best indicate tumors with adverse clinical behavior.

Received February 3, 2003; accepted after revision July 11, 2003.

[1]Division of Diagnostic Radiology, National Cancer Center Hospital and Research Institute, Tsukiji, Chuo-Ku, Tokyo 104-0045, Japan. Address correspondence to U. Tateishi.

[2]Division of Pathology, National Cancer Center Hospital and Research Institute, Tsukiji, Chuo-Ku, Tokyo 104-0045, Japan.

[3]Division of Orthopedics, National Cancer Center Hospital and Research Institute, Tsukiji, Chuo-Ku, Tokyo 104-0045, Japan.

AJR 2004;182:725–731

0361–803X/04/1823–725

Materials and Methods

Patients

We reviewed materials from 36 patients with myxoid–round cell liposarcomas, all of whom who were registered in our pathology files. The clinical details, including follow-up information, were obtained by reviewing all the medical charts. None of the patients was lost to follow-up, which began on the date of primary surgery. The median duration of follow-up was 33 months and ranged from 9 to 276 months. The time to death due to any cause was recorded to determine the overall survival rate.

MRI Studies and Pathologic Correlations

MRI was performed using one of two 1.5-T systems (Horizon, General Electric Medical Systems, Milwaukee, WI; or Visart, Toshiba Medical Systems, Tokyo, Japan). Either the spin-echo or the fast spin-echo technique was used to obtain T1-weighted images (TR range/TE range, 460–720/12–27) in one or more planes (coronal or axial). T2-weighted images (TR range/TE_{eff} range, 3,500–6,000/96–112; echo-train length, 8–12) with flow compensation and presaturation superiorly and inferiorly were then obtained in one or more planes using a body coil. The images were obtained with a field of view of 30–40 cm, an image matrix of 128 × 256, and a slice thickness of 6–10 mm. Gadopentetate dimeglumine was administered IV, and T1-weighted images were obtained in one or more planes with (n = 20) or without (n = 16) fat suppression.

Two radiologists reviewed the MR images, and the findings were reported as a consensus opinion. The lesions were judged according to size, location, depth (superficial or deep), type of margin and contours, internal architecture, presence of a tumor capsule, signal characteristics on T1- and T2-weighted images, and homogeneity (homogeneous or heterogeneous). A superficial tumor (dermal or subcutaneous tumor) was located exclusively above the superficial fascia without invasion of the fascia, whereas a deep tumor was located either exclusively beneath the superficial fascia or superficial to the fascia with invasion of or through the fascia. The signal characteristics were described as isointense or hyperintense relative to the signal intensity of skeletal muscle. The extent (none and weak or pronounced), pattern (globular and nodular or diffuse), and homogeneity of gadolinium-based enhancement were also recorded. Globular and nodular enhancement corresponded to spotty enhancement (range, 3–10 mm) within the mass on contrast-enhanced MR images. Septal structures were categorized as thin (uniform linear structures ≤ 2 mm) or thick (focally thickened linear structures > 2 mm). Tumors containing areas with high-intensity characteristics on both T1- and T2-weighted MR images were considered positive for a high-intensity signal pattern.

Histologic slides of all the patients' tumors were reviewed for diagnosis by an expert pathologist. Immunohistochemical staining was performed in all cases to confirm the diagnosis or tumor type according to the classification system described by Enzinger and Weiss [1]. In this study, the histologic grade of a tumor was determined using a three-grade system established by Hasegawa et al. [15–17]. According to this system, myxoid–round cell liposarcomas are assigned a grade of 1, 2, or 3. Grade 1 tumors (n = 12, 33.3%) are considered low-grade tumors, grade 2 tumors (n = 14, 38.9%) are intermediate-grade tumors, and grade 3 tumors (n = 10, 27.8%) are high-grade tumors (n = 24, 66.7%). Excised specimens were available for review or for mapping correlation with images. Pathology reports were reviewed for descriptive comments characterizing the necrosis and myxoid–round cell tumor components of the lesions.

Statistical Analysis

Patients' demographics and imaging characteristics were compared using Wilcoxon's rank sum test for continuous variables and the chi-square test or Fisher's exact test for categorized variables. Univariate analysis was performed by comparing survival curves generated using the Kaplan-Meier method and carrying out log-rank tests. The relative risk of each variable subjected to multivariate analysis was estimated using a Cox proportional hazards model. All analyses were conducted using SPSS software version 11.0J (Statistical Package for the Social Sciences, Chicago, IL) for Windows (Microsoft, Redmond, WA). Differences and correlations at a p value of less than 0.05 were considered statistically significant.

Results

Twenty-one (58.3%) of the 36 patients were men and 15 were women (41.7%). The mean age at diagnosis was 47 years, and the patients ranged in age from 17 to 87 years. The tumors were located on the lower extremities in 31 patients (86.1%) and the trunk in five (13.9%). The mean tumor size was 9.6 cm, and 16 tumors (44.4%) were larger than 10 cm. Thirty-one tumors (86.1%) were situated deeply, and five (13.9%) were superficial. The surgical procedures consisted of wide excision, amputation, or disarticulation. Surgical margins were confirmed to be adequate at pathology in 28 patients (77.8%). Marginal or intralesional excision with inadequate margins were found in eight (22.2%). Additional treatment included chemotherapy in five patients (13.9%), radiotherapy in nine (25.0%), and both in seven (19.4%).

Metastases occurred in 11 (30.6%) of the 36 patients; the location of metastasis was the peritoneal cavity in five patients (13.9%); soft-tissue in five (13.9%); lung in three (8.3%); and bone, liver, retroperitoneum, and mediastinum in one (2.8%). Eight (38.0%) of the 21 patients who received additional treatment had metastasis subsequently. Twelve (33.3%) of the 36 patients developed local recurrences. Three patients (8.3%) with inadequate excision had local recurrence. Four patients (11.1%) with local recurrence underwent additional therapy.

Ten (27.8%) and 26 (72.2%) of 36 tumors had regular and irregular tumor contours, respectively (Figs. 1–4). Sixteen tumors (44.4%) showed lob-

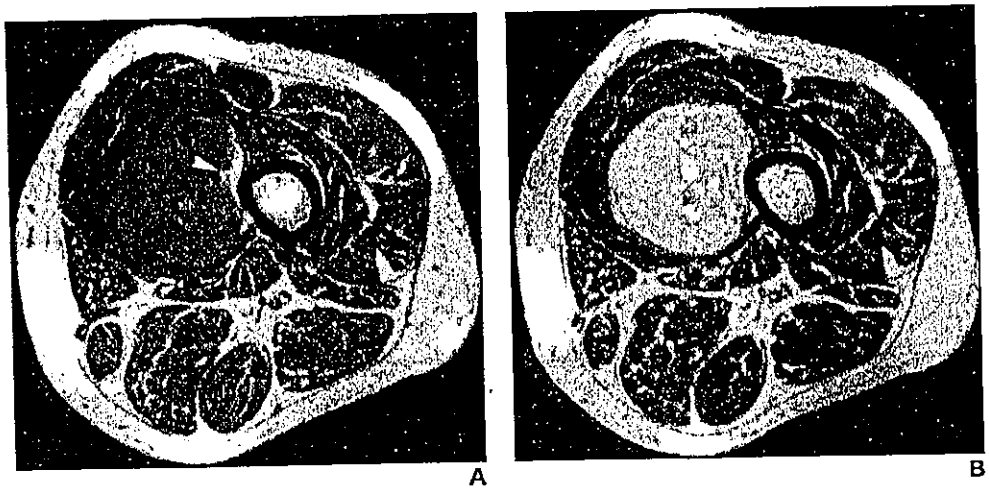

Fig. 1.—38-year-old woman with low-grade myxoid–round cell liposarcoma in left thigh.
A, T1-weighted spin-echo MR image (TR/TE, 720/20) shows tumor has regular contours with small amount of fat signal in periphery (*arrowhead*).
B, Contrast-enhanced T1-weighted spin-echo MR image (720/20) shows diffuse enhancement of tumor.

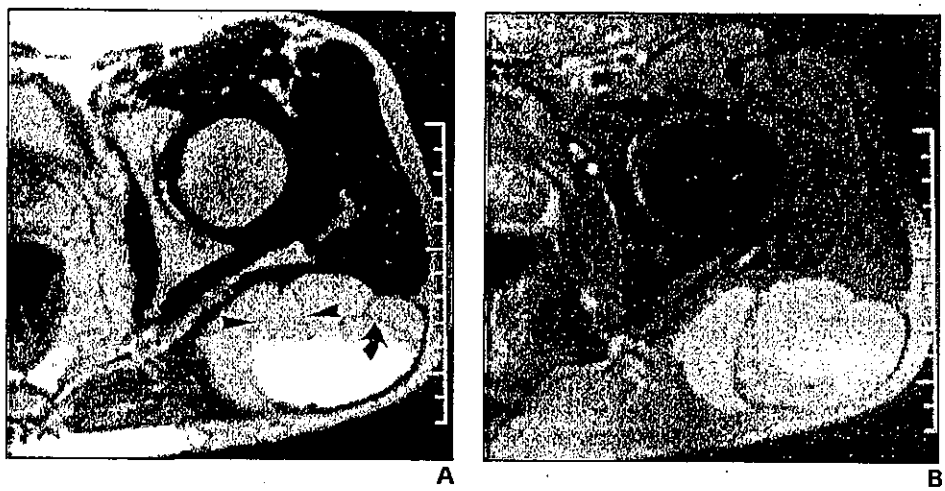

A B

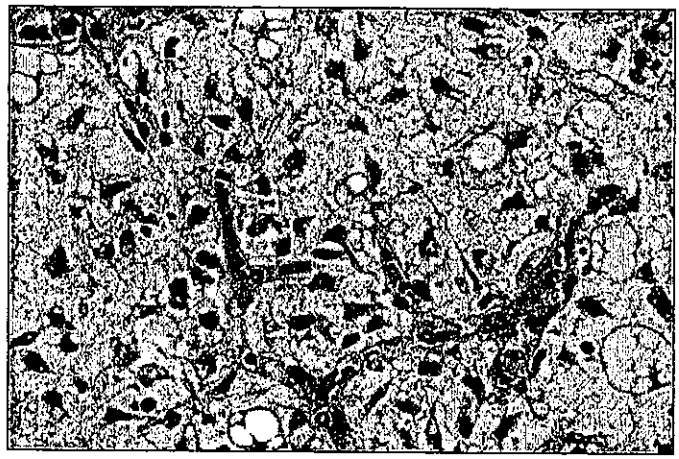

C

Fig. 2.—62-year-old man with low-grade myxoid–round cell liposarcoma in left buttock.
A, Axial T2-weighted fast spin-echo MR image (TR/TE, 3,500/100) shows septate appearance of lesion. Linear structures of low intensity contained thick septa (*arrow*) and thin septa (*arrowheads*).
B, Axial fat-saturated contrast-enhanced T1-weighted spin-echo MR image (720/20) shows tumor of high intensity with slight enhancement of septa.
C, Photomicrograph of specimen shows paucicellular myxoid liposarcoma with less than 25% round cell components has dispersed small round or short spindled cells and multivacuolated lipoblasts within abundant myxoid matrix and plexiform vascular network. (H and E, ×200)

ulated morphology. On MR images, thin and thick septa (Fig. 2) were identified in 31 (86.1%) and 10 (27.8%) tumors, respectively. On T1-weighted MR images the signals of the tumors relative to those of muscle were hyperintense ($n = 15$), isointense ($n = 12$), or hypointense ($n = 9$). Tumors showed predominantly increased signal intensity compared with that of the skeletal muscle on T2-weighted MR images. The images showed the tumor as having a heterogeneous appearance with thin or thick septa of low intensity. High-intensity signals similar to subcutaneous fatty tissue (high-intensity signal pattern) were found in 15 tumors (41.7%) on both T1- and T2-weighted MR images (Figs. 1 and 4).

On contrast-enhanced MR images, pronounced enhancement (Fig. 4) located mostly at the peripheries of the lesions was present in 22 tumors (61.1%). Globular and nodular enhancement (Figs. 3 and 4) was found mostly in the centers of the lesions of 16 patients (44.4%), whereas diffuse enhancement (Fig. 1) was seen in six lesions (16.7%). Contrast-enhanced MR images also revealed that 23 tumors (63.9%) had homogeneously enhanced tumor capsules (Fig. 3).

All tumors were characterized microscopically by a prominent plexiform vascular pattern admixed with an abundant myxoid matrix. The extent of cellularity ranged from slight to moderate, and the lesions were composed of small uniform, round, or spindle-shaped hyperchromatic cells. Tumor necrosis was found on microscopic observation in 12 cases (33.3%). The necrotic areas varied in degree, but most tumors contained only a small amount of necrotic areas that were difficult to identify on MR images.

Statistically significant MRI findings that favored a diagnosis of intermediate- or high-grade tumor were large tumor size (> 10 cm) ($p < 0.01$), deeply situated tumor ($p < 0.05$), tumor possessing irregular contours ($p < 0.001$), absence of lobulation ($p < 0.001$), absence of thin septa ($p < 0.05$), presence of thick septa ($p < 0.01$), absence of tumor capsule ($p < 0.001$), high-intensity signal pattern ($p < 0.01$), pronounced enhancement ($p < 0.001$), and globular and nodular enhancement ($p < 0.001$). The presence of thin septa or a tumor capsule indicates low-grade tumor. Irregular contours were found in only 10 high-grade tumors (58.8%). All the low-grade tumors had a capsule, thin septa, and a high-intensity signal pattern. The odds ratios for a specific finding favoring a diagnosis of intermediate- or high-grade tumor are shown in Table 1. The multiple logistic regression model showed that irregular contour and thick septa were the most significant predictors of intermediate- or high-grade tumors, with an odds ratio of 13.8 for both (95% confidence interval [CI], 1.5–128.8; $p < 0.05$).

At the last follow-up, 10 (27.8%) of the 36 patients had died of their disease and four (11.1%) were alive with metastatic disease. The 5- and 10-year survival rates were 80.5%

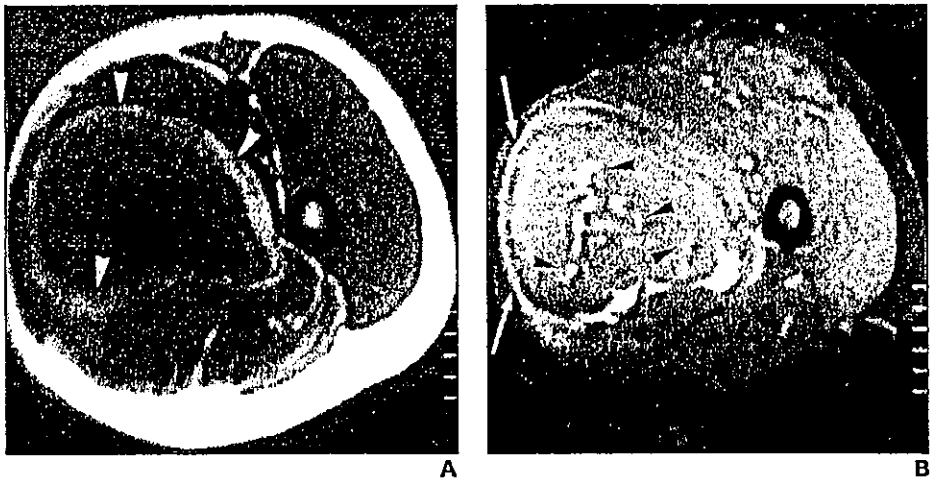

A B

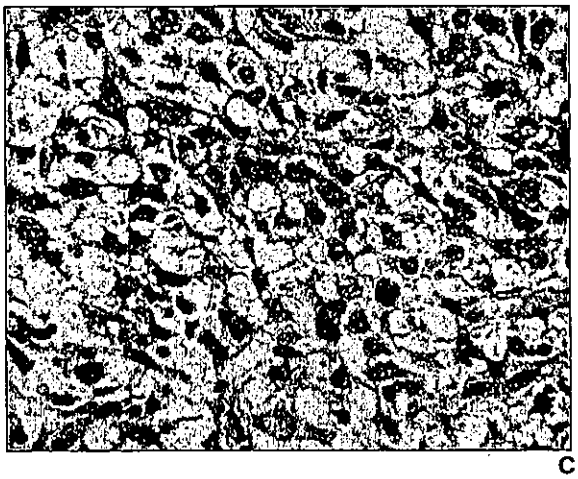

C

Fig. 3.—28-year-old man with intermediate-grade myxoid–round cell liposarcoma in left thigh.
A, Axial T1-weighted spin-echo MR image (TR/TE, 650/12) shows high-intensity signal pattern (*arrowheads*) in periphery of tumor.
B, Fat-suppressed contrast-enhanced T1-weighted spin-echo MR image (650/12) shows pseudocapsular enhancement (*arrows*) and globular and nodular enhancement (*arrowheads*).
C, Photomicrograph of specimen shows cellular myxoid liposarcoma with round cell components composed of solid sheets of round cells with large and coarse chromatin and little intervening myxoid stroma. (H and E, ×200)

and 72.4%, respectively. The univariate analysis showed that thin septa ($p < 0.05$), tumor capsule ($p < 0.01$), and pronounced enhancement ($p < 0.01$) were significantly associated with overall survival (Table 2). The multivariate analysis revealed that pronounced enhancement was the most significant adverse prognostic factor (Fig. 5) with a relative risk of 7.3 (95% CI, 1.5–35.1; $p < 0.05$).

TABLE 1 Odds Ratio for Features Favoring Diagnosis of Intermediate- or High-Grade Myxoid–Round Cell Liposarcoma

Feature	Odds Ratio	95% CI
Size > 10 cm	9.0	2.6–30.9
Lobulation absent	21.0	8.3–126.5
Thick septa present	20.3	2.1–188.7
Pronounced enhancement present	34.7	3.72–324.1
Globular and nodular enhancement present	9.0	2.0–41.3

Note.—CI = confidence interval.

Discussion

In this study, we documented the prognostic significance of MRI features in patients with myxoid–round cell liposarcomas. Univariate analysis revealed that the presence of thin septa, a tumor capsule, and pronounced enhancement had a significant correlation with overall survival. Multivariate analysis showed that, of these variables, pronounced enhancement on contrast-enhanced MR images was the most influential adverse prognostic factor. This MRI finding of enhancement correlated with the round cell–component content on pathologic specimens. The prognostic importance of the round cell component has been acknowledged in previous studies [18–20]. From a practical viewpoint, detection of this enhancement pattern on contrast-enhanced MR images in myxoid–round cell liposarcomas is useful for predicting their behavior.

The amount of necrosis has been reported to be correlated with clinical outcome [21–25]. Spontaneous tumor necrosis identified in four (4%) of 95 patients with myxoid–round cell liposarcomas was correlated with increased risks of metastasis and death [18]. In our study, we did not evaluate the relationship between the presence of tumor necrosis and patient prognosis, because most tumors accompanied by necrosis in our study contained only a small amount of necrotic areas that were difficult to identify on MR images.

On contrast-enhanced MR images, pronounced enhancement was located mainly at the periphery of the lesion in 61.1% of the pa-

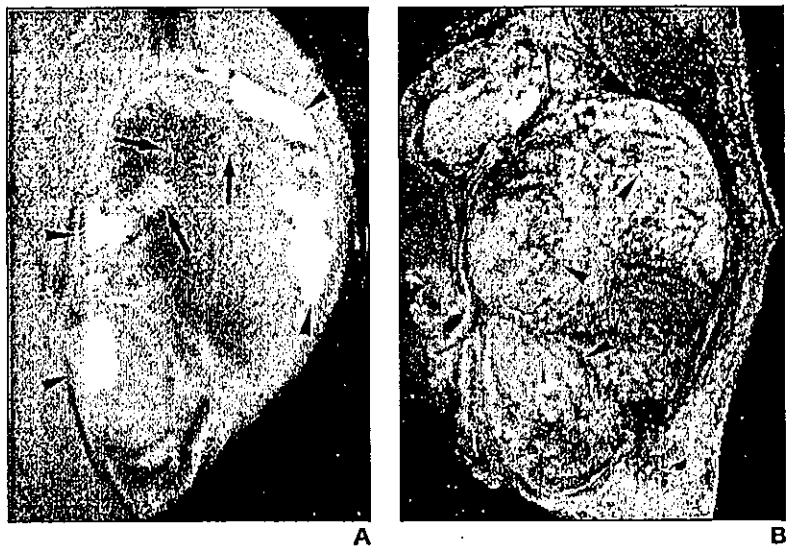

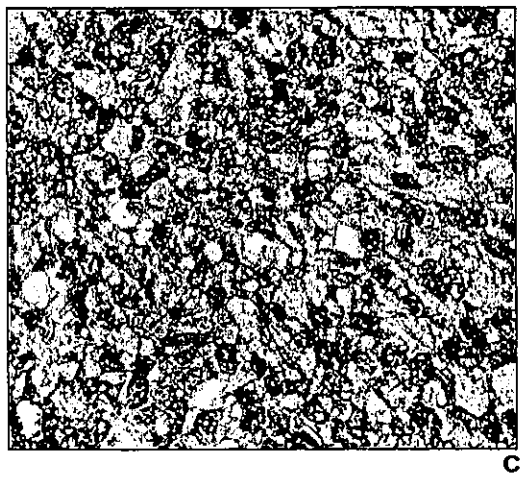

Fig. 4.—69-year-old man with high-grade myxoid–round cell liposarcoma in left thigh.
A, Sagittal contrast-enhanced T1-weighted spin-echo MR image (TR/TE, 600/15) shows globular and nodular enhancement (*arrows*) and pronounced enhancement (*arrowheads*) predominantly at tumor periphery.
B, Photograph of macroscopic specimen of same tumor as in A shows heterogeneous tumor components (*arrowheads*).
C, Photomicrograph shows that specimen is composed of solid sheets of uniform round cells with large and coarse chromatin. (H and E, ×200)

tients, and globular and nodular enhancement occurred at the lesion center in 44.4%. These two patterns of enhancement were characteristic of intermediate- or high-grade tumors. Round cell components were reported to be located at the peripheries of lobules; adjacent to fibrous septa extending through the tumor; and surrounding large vessels, particularly in tumors with only a small amount of round cell components [7, 8]. Thus, these two enhancement patterns may be reliable imaging findings for detecting round cell components within tumors. In one study, despite a small sample size, researchers showed that patients (n = 5) who initially had a tumor with 5% or greater round cell components had a significantly higher incidence of metastasis or death from disease than those (n = 7) who initially had a tumor with less than 5% round cell components [18]. In a study of 24 patients with round cell components composing 25% or more of the tumor, round cell components were associated significantly with a lower survival rate [19]. However, the correlation between the quantity of round cell components and the clinical outcome may depend on the difficulty in quantifying the round cell components at transitional areas at microscopic observation.

There was no significant difference between the risks of an adverse outcome in patients with myxoid and transitional areas without round cell components and those with myxoid areas alone [19]. The pathologic variables responsible for differences among observers in identifying round cell components are considered to be numerous and include inaccurate criteria for tissue processing and selection of the assessment area within the spectrum of myxoid–round cell liposarcomas [20]. Our results suggest that contrast-enhanced MR images can assist in detecting round cell component content within the entire tumor and assist in the distinction of low-grade and of intermediate- or high-grade myxoid–round cell liposarcomas.

In previous reports [26–29], the descriptions of the enhancement patterns identified on MR images included little enhancement or a few patterns (i.e., heterogeneous, homogeneous, no enhancement). However, the end points selected in these prior studies depended simply on the pathologic diagnosis of "myxoid liposarcoma," and the investigators were unaware of the lineage of "myxoid–round cell liposarcoma" as a disease entity. The results of our study are based on a definite diagnosis of myxoid–round cell liposarcoma, and we stress that

TABLE 2 MRI Findings and Univariate Analyses of Survival in 36 Cases of Myxoid–Round Cell Liposarcoma

MRI Findings	No. (%) of Cases	5-Year Survival Rate (%)	p^a
Size (cm)			0.10
≤ 10	20 (55.6)	84.2	
> 10	16 (44.4)	56.8	
Depth			0.26
Superficial	5 (13.9)	100	
Deep	31 (86.1)	66.7	
Contour			0.27
Regular	26 (72.2)	71.2	
Irregular	10 (27.8)	62.5	
Lobulation			0.19
Absent	20 (55.6)	59.8	
Present	16 (44.4)	85.2	
Thin septa			0.02
Absent	5 (13.9)	26.7	
Present	31 (86.1)	77.1	
Thick septa			0.47
Absent	26 (72.2)	66.7	
Present	10 (27.8)	72.3	
Tumor capsule			< 0.01
Absent	13 (36.1)	16.6	
Present	23 (63.9)	83.1	
Pronounced enhancement			< 0.01
Absent	14 (38.9)	100	
Present	22 (61.1)	54.9	
Globular and nodular enhancement			0.91
Absent	20 (55.6)	78.4	
Present	16 (44.4)	66.8	
High-Intensity signal pattern			0.71
Absent	21 (58.3)	72.4	
Present	15 (41.7)	69.1	

[a]Log-rank test.

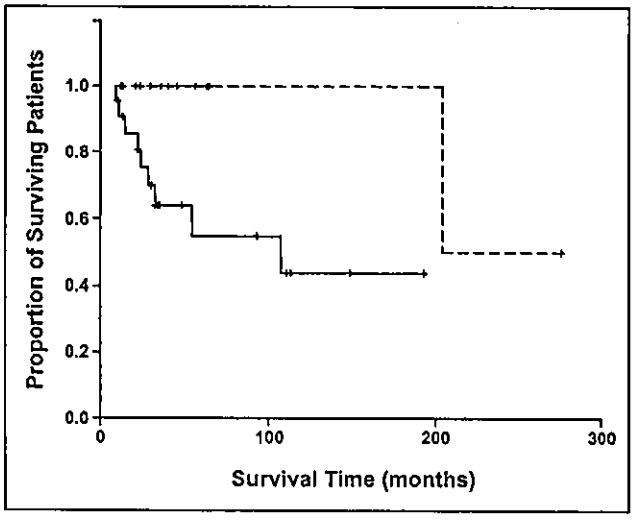

Fig. 5.—Graph shows Kaplan-Meier survival curve according to presence (*solid line*) or absence (*dashed line*) of pronounced enhancement on contrast-enhanced MR images for 36 patients with myxoid–round cell liposarcomas.

the presence of globular and nodular or pronounced enhancement identified on MRI is a finding suggestive of intermediate- or high-grade tumor and reflects the amount of round cell components in the tumor, which strongly affects patient outcome.

The presence of linear or amorphous hyperintense foci behaving like fatty tissue on T1-weighted MR images has been reported to be a pattern suggestive of myxoid liposarcoma [27]. Myxoid–round cell liposarcoma often consists of multiple histologic subtypes in the same lesion. We observed a high-intensity signal pattern in 15 low-grade tumors, and this finding was consistent with immature fatty tissue or the fat components of the tumors. Immature spindle cells lacking obvious fat genesis may be seen next to multivacuolated lipoblasts. Although MRI is sensitive enough to detect minute fat deposits or immature fatty components, our univariate analysis showed no significant association between high-intensity signal pattern on MR images and survival [28, 29].

In summary, the spectrum of MRI findings in myxoid–round cell liposarcomas is continuous. MRI findings can assist in the distinction between low-grade and intermediate- or high-grade myxoid–round cell liposarcomas. MRI findings that favored a diagnosis of intermediate- or high-grade tumor included large (> 10 cm) size of tumor, deeply situated tumor, tumor possessing irregular contours, absence of lobulation, absence of a tumor capsule, absence of thin septa, presence of thick septa, high-intensity signal pattern, pronounced enhancement, and globular and nodular enhancement. The presence of thin septa or a tumor capsule indicates low-grade tumor. Imaging features associated with overall survival were thin septa, a tumor capsule, and pronounced enhancement. Multivariate analysis showed that pronounced enhancement on MRI is the most significant factor in predicting an adverse prognosis for patients with myxoid–round cell liposarcoma.

References

1. Enzinger FM, Weiss SW. *Soft tissue tumors*, 4th ed. St. Louis, MO: Mosby–Year Book, 2001: 670–687
2. Enzinger FM, Winslow DJ. Liposarcoma: a study of 103 cases [in German]. *Virchows Arch Path Anat Physiol Klin Med* 1962;335:367–388
3. Evans HL. Liposarcoma: a study of 55 cases with a reassessment of its classification. *Am J Surg Pathol* 1979;3:507–523
4. Evans HL. Liposarcomas and atypical lipomatous tumors: a study of 66 cases followed for a minimum of 10 years. *Surg Pathol* 1988;1:41–54

5. Hashimoto H, Enjoji M. Liposarcoma: a clinicopathologic subtyping of 52 cases. *Acta Pathol Jpn* 1982;32:933–948
6. Knight JC, Renwick PJ, Cin PD, Van den Berghe H, Fletcher CD. Translocation t(12;16)(q13;p11) in myxoid and round cell liposarcoma: molecular and cytogenetic analysis. *Cancer Res* 1995;55:24–27
7. Panagopoulos I, Mandahl N, Ron D, et al. Characterization of the *CHOP* breakpoints and fusion transcripts in myxoid liposarcomas with the 12;16 translocation. *Cancer Res* 1994;54:6500–6503
8. Kuroda M, Ishida T, Horiuchi H, et al. Chimeric *TLS/FUS-CHOP* gene expression and the heterogeneity of its junction in human myxoid and round cell liposarcoma. *Am J Pathol* 1995;147: 1221–1227
9. Hisaoka M, Tsuji S, Morimitsu Y, et al. Detection of *TLS/FUS-CHOP* fusion transcripts in myxoid and round cell liposarcomas by nested reverse transcription-polymerase chain reaction using archival paraffin-embedded tissues. *Diagn Mol Pathol* 1998;7:96–101
10. Jelinek JS, Kransdorf MJ, Shmookler BM, Aboulafia AJ, Malawer MM. Liposarcoma of the extremities: MR and CT findings in the histologic subtypes. *Radiology* 1993;186:455–459
11. London J, Kim EE, Wallace S, Shirkhoda A, Coan J, Evans H. MR imaging of liposarcomas: correlation of MR features and histology. *J Comput Assist Tomogr* 1989;15:832–835
12. Sundaram M, Baran G, Merenda G, McDonald DJ. Myxoid liposarcoma: MR imaging appearances with clinical and histological correlation. *Skeletal Radiol* 1990;19:359–362
13. Ramsdell MG, Chew FS, Keel SB. Myxoid liposarcoma of the thigh. *AJR* 1998;170:1242
14. Sung MS, Kang HS, Suh JS, et al. Myxoid liposarcoma: appearance at MR imaging with histologic correlation. *RadioGraphics* 2000;20:1007–1019
15. Hasegawa T, Yokoyama R, Lee YH, et al. Prognostic relevance of a histological grading system using MIB-1 for adult soft-tissue sarcoma. *Oncology* 2000;58:66–74
16. Hasegawa T, Yamamoto S, Yokoyama R, et al. Prognostic significance of grading and staging systems using MIB-1 score in adult patients with soft tissue sarcoma of the extremities and trunk. *Cancer* 2002;95:843–851
17. Hasegawa T, Yamamoto S, Nojima T, et al. Validity and reproducibility of histologic diagnosis and grading for adult soft-tissue sarcomas. *Hum Pathol* 2002;33:111–115
18. Kilpatrick SE, Doyon J, Choong PFM, et al. The clinicopathologic spectrum of myxoid and round cell liposarcoma: a study of 95 cases. *Cancer* 1996;77:1450–1458
19. Smith TA, Easley KA, Goldblum JR. Myxoid/round cell liposarcoma of the extremities: a clinicopathologic study of 29 cases with particular attention to extent of round cell liposarcoma. *Am J Surg Pathol* 1996;20:171–180
20. Antonescu CR, Tschernyavsky SJ, Decuseara R, et al. Prognostic impact of p53 status, *TLS-CHOP* fusion transcript structure, and histological grade in myxoid liposarcoma: molecular and clinicopathologic study of 82 cases. *Clin Cancer Res* 2001;7:3977–3987
21. Lack EE, Steinberg SM, White DM, et al. Extremity soft tissue sarcomas: analysis of prognostic variables in 300 cases and evaluation of tumor necrosis as a factor in stratifying high-grade sarcomas. *J Surg Oncol* 1989;41:263–273
22. Mandard AM, Petiot JF, Marnay J, et al. Prognostic factors in soft tissue sarcomas: a multivariate analysis of 109 cases. *Cancer* 1989;63:1437–1451
23. Choong PFM, Gustafson P, Willen H, et al. Prognosis following locally recurrent soft tissue sarcoma: a staging system based on primary and recurrent tumor characteristics. *Int J Cancer* 1995;60:33–37
24. Orson GG, Sim FH, Reiman HM, et al. Liposarcoma of the musculoskeletal system. *Cancer* 1987;60:362–370
25. Reitan JB, Kaazhus O, Brenhoud IO, et al. Prognostic factors in liposarcoma. *Cancer* 1985;55: 2482–2490
26. Arkun R, Memis A, Akalin T, Ustun EE, Sabah D, Kandiloglu G. Liposarcoma of soft tissue: MRI findings with pathologic correlation. *Skeletal Radiol* 1997;26:167–172
27. Munk PL, Lee MJ, Janzen DL, et al. Lipoma and liposarcoma: evaluation using CT and MR imaging. *AJR* 1997;169:589–594
28. Kransdorf MJ. Malignant soft tissue tumors in a large referral population: distribution of diagnoses by age, sex, and location. *AJR* 1995;164: 129–134
29. Kransdorf MJ, Murphey MD. Radiologic evaluation of soft-tissue masses: a current perspective. *AJR* 2000;175:575–587

The reader's attention is directed to the article titled "Lipomas, Lipoma Variants, and Well-Differentiated Liposarcomas (Atypical Lipomas): Results of MRI Evaluations of 126 Consecutive Fatty Masses," which appears on page 733.

Histopathology 2004, 44, 297–306

Correspondence

Gastric glomangiomyoma: a pedunculated extramural mass with a florid angiomyomatous pattern

Sir: Glomus tumours are uncommon mesenchymal tumours with an incidence of about 1.6% among soft tissue tumours. The tumours are most commonly found in the peripheral soft tissues, especially in the distal parts of the extremities.[1] Here, we describe a rare variant of the glomus tumour, glomangiomyoma, in the gastrointestinal tract with an unusual extramural location and a florid smooth muscle cell component.

A 54-year-old Chinese woman presented with recurrent epigastric pain for 2 years. Repeated endoscopies revealed no mucosal lesion but only vague bulging in the posterior wall of the gastric antrum. Computed axial tomography revealed a well-defined, 70-mm paragastric solid mass in the right upper abdomen connected to the stomach by a narrow stalk, extending just inferior to the liver to the level of the aortic bifurcation. The tumour was surgically removed and she has remained well during the last 3 months of follow-up after the operation.

The tumour was a circumscribed ovoid mass weighing 101 g and measuring 70 × 60 × 35 mm with a solid tan-coloured cut surface (Figure 1A). There was no capsule, but the external surface of the tumour was smooth and covered by peritoneum.

Microscopically, the tumour showed a biphasic pattern (Figure 1B). The predominant component was eosinophilic spindle cells whorling around mostly capillary-sized vessels, forming an angiomyoma-like pattern (Figure 1C). These cells were strongly positive for smooth muscle markers including desmin (Figure 1D), smooth muscle actin and muscle-specific actin. The other component was the diagnostic glomus cells, comprising islands and sheets of small ovoid cells surrounding gapped or staghorn-like vessels. These cells possessed well-demarcated round basophilic nuclei and scanty cytoplasm (Figure 1E). Collagen IV and reticulin showed pericellular staining patterns around these cells. Only a few of these cells were positive for desmin (Figure 1F). Both components showed negative staining for AE1/AE3, CD34, C-kit (CD117), S100, HMB45, chromogranin and synaptophysin. Neither necrosis nor cytological atypia were present. The proliferative index of the tumour was low with rare mitotic figures (<1 per 50 high-power fields) and low MIB-2 (Ki67) staining (<1% for both cell components).

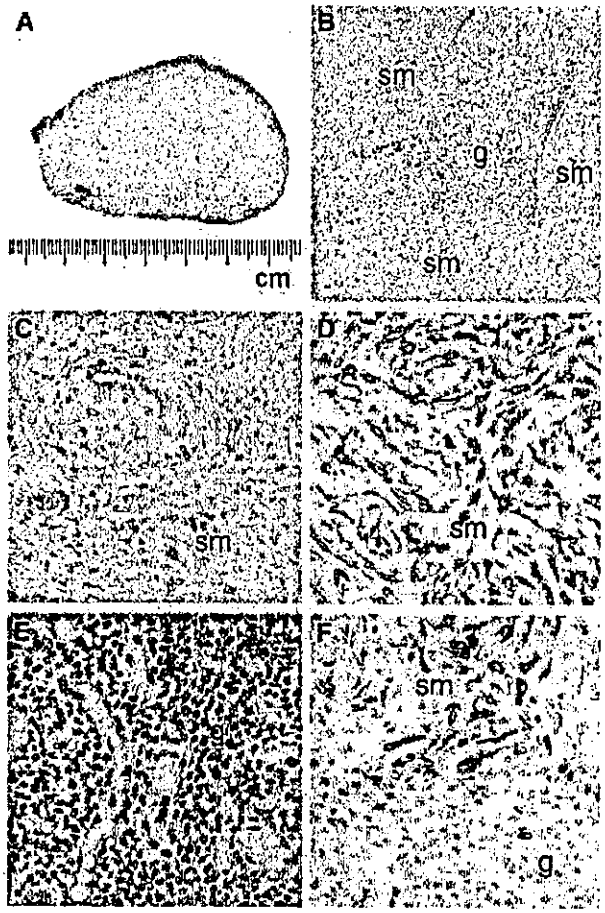

Figure 1. A, Gross appearance of the solid tan-coloured cut surface of the glomangiomyoma. B, Low-power view of H–E section showing a small island of the basophilic ovoid glomus tumour cells (g) surrounded by the abundant smooth muscle cell component (sm). C, High-power view of H–E section showing the whorling pattern of the smooth muscle cells (sm) around vessels. D, Immunostaining of desmin (Dako M760, clone D33, dilution 1 : 150) showing the angiomyomatous pattern of this tumour with the strong staining of the smooth muscle cells (sm). E, High-power view of the H–E section showing the pericytoma-like glomus tumour cell component (g). F, Immunostaining of desmin showing the transition from negatively stained glomus tumour cells (g) to strongly stained smooth muscle cells (sm).

In conclusion, the tumour was a pedunculated, subsersosal gastric glomangiomyoma with a predominant spindled smooth muscle cell component, resulting in a striking angiomyomatous pattern. The tell-tale glomus cell component was only confined to scattered small areas. Glomus tumours have a close growth association with vessels. Variable degrees of differentiation/transformation towards mature smooth muscle cells and a

focal angiomyomatous pattern have previously been described.[1,2] A predominant spindle cell component, as in the present case, however, has not been reported. Accordingly, differential diagnoses include gastrointestinal stromal cell tumour, haemangiopericytoma, solitary fibrous tumour, leiomyoma/leiomyoma of uncertain malignant potential, schwannoma and angiomyolipoma (see Ref. 3 for review).

Miettinen and coworkers[3] reviewed the largest series of 32 gastrointestinal glomus tumours. Most of them were circumscribed, intramural or intraluminal masses located in the gastric antrum. Typically, the presenting symptoms were those of gastrointestinal bleeding or ulcers. Most tumours were small and the patients fared well, except one with a large tumour (65 mm in size), who developed disease metastatic to the liver. The prognostic criteria of gastrointestinal glomangiomyoma or glomus tumours as a whole are not well established. With regard to the large size (70 mm) of the tumour of our patient, long-term follow-up is warranted. For glomus tumour affecting the extremities, location of the tumour in a deeper tissue plane is associated with a poorer prognosis.[4] The depth of primary tumour, however, does not seem to play a significant role in the prognosis for gastrointestinal glomus tumour.[3] Spindle cells in glomus tumours have been suggested to be associated with an adverse prognosis.[3,4] However, it should be noted that among the few unfavourable cases reported, the 'spindle' cells were mostly sarcoma-like, resembling malignant fibrous histiocytoma or leiomyosarcoma.[4] Thus, whether the cytologically bland, spindled smooth muscle component in the present case plays an additional adverse role in the clinical behaviour remains doubtful.

A W I Lo
L T C Chow
K F To
M Y Yu

Department of Anatomical and Cellular Pathology, The Chinese University of Hong Kong, Prince of Wales Hospital, Shatin, New Territories, Hong Kong Special Administration Region, People's Republic of China

1. Weiss SW, Goldblum JR. Perivascular tumors. In Weiss SW, Goldblum JR eds. *Enzinger and Weiss's soft tissue tumours*, 4th edn. St Louis: Mosby, Inc., 2001; 985–1036.
2. Miliauskas JR, Worthley C, Allen PW. Glomangiomyoma (glomus tumour) of the pancreas: a case report. *Pathology* 2002; 34; 193–195.
3. Miettinen M, Paal E, Lasota J, Sobin LH. Gastrointestinal glomus tumours. A clinicopathologic, immunohistochemical, and molecular genetic study of 32 cases. *Am. J. Surg. Pathol.* 2002; 26; 301–311.
4. Folpe AL, Fanburg-Smith JC, Miettinen M, Weiss SW. Atypical and malignant glomus tumors. Analysis of 52 cases, with a proposal for the reclassification of glomus tumors. *Am. J. Surg. Pathol.* 2001; 25; 1–12.

Gastrointestinal zygomycosis: two case reports

Sir: Gastrointestinal zygomycosis is rare. We present one case of small intestinal mucormycosis and one case of colonic and hepatic entomophthoromycosis, documenting the dramatically different clinicopathological features caused by fungi of the two orders of the class *Zygomycetes*.

A 65-year-old Caucasian man with chronic obstructive pulmonary disease admitted with lobar pneumonia rapidly developed respiratory and renal failure. Subsequently, he had a major rectal bleed and emergency extended right hemicolectomy revealed four separate well-demarcated perforations within otherwise normal ileum.

Microscopy showed florid acute inflammation and microabscesses at the perforation sites, associated with abundant multinucleate giant cells (Figure 1). Within the luminal necrotic debris and multinucleate giant cells were abundant irregularly shaped, non-septate hyphae, branching at right angles, morphologically consistent with *Mucorales*. Post-operatively, he was treated with 4 weeks of intravenous amphotericin B. Two years later, he is alive and well.

The second case was a 45-year-old Iranian farmer admitted with right iliac fossa pain. Computed tomography and subsequent right hemicolectomy revealed a 90-mm solid caecal mass which histologically was a caecal abscess containing a striking number of eosinophils, multinucleated giant cells and multiple broad and sparsely septate fungal hyphae surrounded by characteristic 'Splendore–Hoeppli' precipitates (Figure 2). Six weeks later he developed multiple liver abscesses and fine needle aspiration again showed *Entomophthorales* hyphae surrounded by 'Splendore–Hoeppli' precipitates. Treatment with ketaconazole, together with cotrimoxazole, was successful and he was discharged 4 weeks later.

Mucorales and *Entomophthorales*, the two orders of the class *Zygomycetes*, are closely related fungi but have dramatically different disease manifestations.[1] *Mucorales* are opportunistic fungi that cause rapidly disseminating, acute fulminating and often fatal infections in diabetic, debilitated or immunocompromised hosts.[2] Fungi tend to invade blood vessels causing

Figure 1. Small-bowel mucormycosis. Microabscesses and multinucleate giant cells containing *Mucorales* (inset).

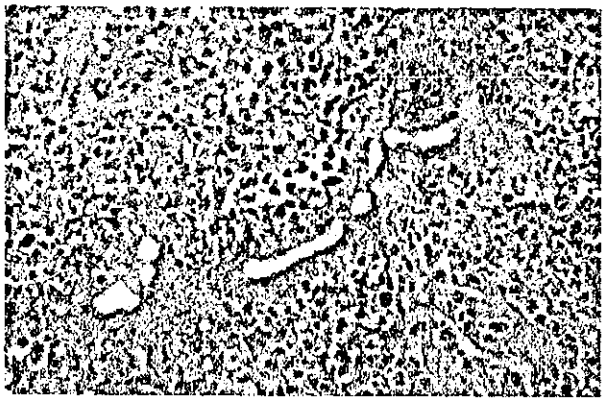

Figure 2. 'Splendore–Hoeppli' precipitate in entomophthoromycosis.

mycotic emboli. Gastrointestinal mucormycosis is rare, with small intestinal involvement in immunocompetent adults described in only five cases in the literature, all of which were fatal, due to late diagnosis.

Entomophthorales are ubiquitous fungi causing generally chronic, subcutaneous or nasofacial infections in immunocompetent individuals in tropical and subtropical regions. The hyphae show no tendency for invading blood vessels.

Our first patient was severely debilitated with chronic obstructive pulmonary disease and chest infection and had received multiple different antibiotics prior to surgery, which probably predisposed to the fungal infection, perhaps via ingestion of fungus and invasion from the lumen into the intestinal wall. No apparent underlying intestinal disease was identifiable.

It is not possible to differentiate the various mucormycoses in tissue sections and isolation of *Mucorales* is difficult; material has to be cultured immediately.[3] Fungal cultures were not performed for our first patient. However, morphologically the appearances of the fungus were consistent with *Mucorales* and the tissue macroscopy and histology characteristic of this infection. Although Aspergillus can occasionally produce a similar tissue reaction with multinucleated giant cells, it is readily distinguished by narrow hyphae with dichotomous branching at acute angles.

Entomophthoromycosis is histologically characterized by broad, branching and sparsely septate hyphae surrounded by 'Splendore–Hoeppli' precipitates. This microscopic picture is diagnostic and distinguishes entomophthoromycosis from other fungal infections, including mucormycosis. However, culture is necessary for species identification. The eosinophilic, periodic acid–Schiff-positive material of the 'Splendore–Hoeppli' phenomenon consists mainly of immune complexes and is an expression of the host immune response.

Fifteen cases of gastrointestinal entomophthoromycosis have been reported to date, with liver involvement in only two cases.[4,5] Organisms, whenever identified, have been *Basidiobolus haptosporus*.[6] Our second patient was a farmer without any evidence of immune deficiency, systemic illness or subcutaneous lesion. We suspect that ingestion of fungi led to abscess formation in the caecum, and the hemicolectomy introduced fungi into the lymphatic and/or portal venous systems resulting in hepatic abscesses. Species identification was impossible because attempts at blood and liver aspirate cultures were unsuccessful.

Treatment of Zygomycoses requires aggressive metabolic support, antifungal therapy and surgical resection and/or debridement of necrotic involved tissue. Early diagnosis, by histological examination, is important so that life-saving antifungal therapy can be initiated.

B Azadeh
D O'B McCarthy[1]
A Dalton[2]
F Campbell

Department of Pathology, Royal Liverpool University Hospital, Liverpool, and [1]Departments of Surgery and [2]Pathology, Glan Clwyd Hospital, Denbighshire, UK

1. Ribes JA, Vanover-Sams CL, Baker DJ. Zygomycetes in human disease. *Clin. Microbiol. Rev.* 2000; 13; 236–301.

2. Lyon DT, Schubert TT, Mantia AG *et al.* Phycomycosis of the gastrointestinal tract. *Am. J. Gastroenterol.* 1979; 72; 379–394.
3. Alspaugh JA, Perfect JR. Infections due to zygomycetes and other rare fungal opportunities. *Sem. Resp. Crit. Care Med.* 1997; 18; 265–279.
4. Bittencourt AL, Ayala MAR, Ramos EAG. A new form of zygomycosis different from mucormycosis: report of two cases and review of the literature. *Am. J. Trop. Med. Hyg.* 1979; 28; 564–569.
5. de Aguiar E, Moraes WC, Londero AT. Gastrointestinal entomophthoromycosis caused by *B. haptosporus*. *Mycopathologia* 1980; 72; 101–105.
6. Lyon GM, Smilack JD, Komatsu KK *et al.* Gastrointestinal basidiobolomycosis in Arizona: clinical and epidemiological characteristics and review of the literature. *Clin. Infect. Dis.* 2001; 32; 1448–1455.

Unusually close association of ectopic intrathyroidal parathyroid gland and papillary microcarcinoma of the thyroid

Sir: We here report the unusual case of a papillary microcarcinoma of the left thyroid lobe in close proximity to an ectopic intrathyroidal parathyroid gland. A bilateral nodal goitre had been removed from a 41-year-old woman. Clinically, an adenoma was suspected within the left lobe, and the right lobe showed a nodule with decreased hormonal function ('cold' nodule) on scintigraphic evaluation. There was no history of hyperparathyroidism.

On gross examination, the largest diameters of the two roughly spindle-shaped thyroid lobes were 62 and 48 mm. Cut surfaces revealed multiple nodules measuring up to 25 mm in largest diameter. Histological analysis showed the typical picture of a '*struma colloides nodosa*' with focal regressive changes. However, the left-sided lobe contained an unusual histological finding with the close association of an encapsulated papillary microcarcinoma (follicular variant, maximum diameter 7 mm) and an ectopic (intrathyroidal) parathyroid gland (Figure 1a).

The papillary microcarcinoma showed characteristic cytological features with crowding and a ground-glass appearance of the nuclei (Figure 1b) but a completely follicular microarchitecture ('follicular variant of papillary carcinoma of the thyroid').

Immunohistochemically, the parathyroid gland revealed a typical endocrine phenotype with expression of synaptophysin (Figure 1c). The papillary carcinoma strongly expressed S100 protein, while in the adjacent normal thyroid and the parathyroid only a few scattered reticulum cells were reactive with the anti-S100 antibody (Figure 1d).

The intrathyroidal localization of parathyroid glands in general seems to be a rare finding, but there are varying reports as to its true incidence. In several studies, some of which were concerned with surgery for primary hyperparathyroidism, the frequency of intrathyroidal parathyroid glands ranged from 2.4%[1] to 8%.[2–6]

The incidence of occult papillary carcinoma in young adults (20–40 years) was 3% in an autopsy study of 138 patients.[7] In people over 40 years of age, however, this incidence increases, leading to an overall incidence of 5–24% in the whole population.[8,9]

Thus, the present case of occult papillary microcarcinoma in close proximity to an intrathyroidal parathyroid gland is a most unusual incidental finding.

H-W Bernd
H-P Horny

Institut für Pathologie,
Universitätsklinikum Schleswig-Holstein,
Lübeck, Germany

1. Lee NJ, Blakey JD, Bhuta S, Calcaterra TC. Unintentional parathyroidectomy during thyroidectomy. *Laryngoscope* 1999; 109; 1238–1240.
2. Rodriquez JM, Tezelman S, Siperstein AE *et al.* Localization procedures in patients with persistent or recurrent hyperparathyroidism. *Arch. Surg.* 1994; 129; 870–875.
3. Feliciano DV. Parathyroid pathology in an intrathyroidal position. *Am. J. Surg.* 1992; 164; 496–500.
4. Proye C, Bizard JP, Carnaille B, Quievreux JL. Hyperparathyroidism and intrathyroid parathyroid gland. 43 cases. *Ann. Chir.* 1994; 48; 501–506.
5. McIntyre RC, Eisenach JH, Pearlman NW, Ridgeway CE, Liechty RD. Intrathyroidal parathyroid glands can be a cause of failed cervical exploration for hyperparathyroidism. *Am. J. Surg.* 1997; 174; 750–753; discussion 753–754.
6. Harach HR, Vujanic GM. Intrathyroidal parathyroid. *Pediatr. Pathol.* 1993; 13; 71–74.
7. Komorowski RA, Hanson GA. Occult thyroid pathology in the young adult: an autopsy study of 138 patients without clinical thyroid disease. *Hum. Pathol.* 1988; 19; 689–696.
8. Martinez-Tello FJ, Martinez-Cabruja R, Fernandez-Martin J, Lasso-Oria C, Ballestin-Carcavilla C. Occult carcinoma of the thyroid. A systematic autopsy study from Spain of two series performed with two different methods. *Cancer* 1993; 71; 4022–4029.
9. Fink A, Tomlinson G, Freeman J-L, Rosen IB, Asa SL. Occult micropapillary carcinoma associated with benign follicular thyroid disease and unrelated thyroid neoplasms. *Mod. Pathol.* 1996; 9; 816–820.

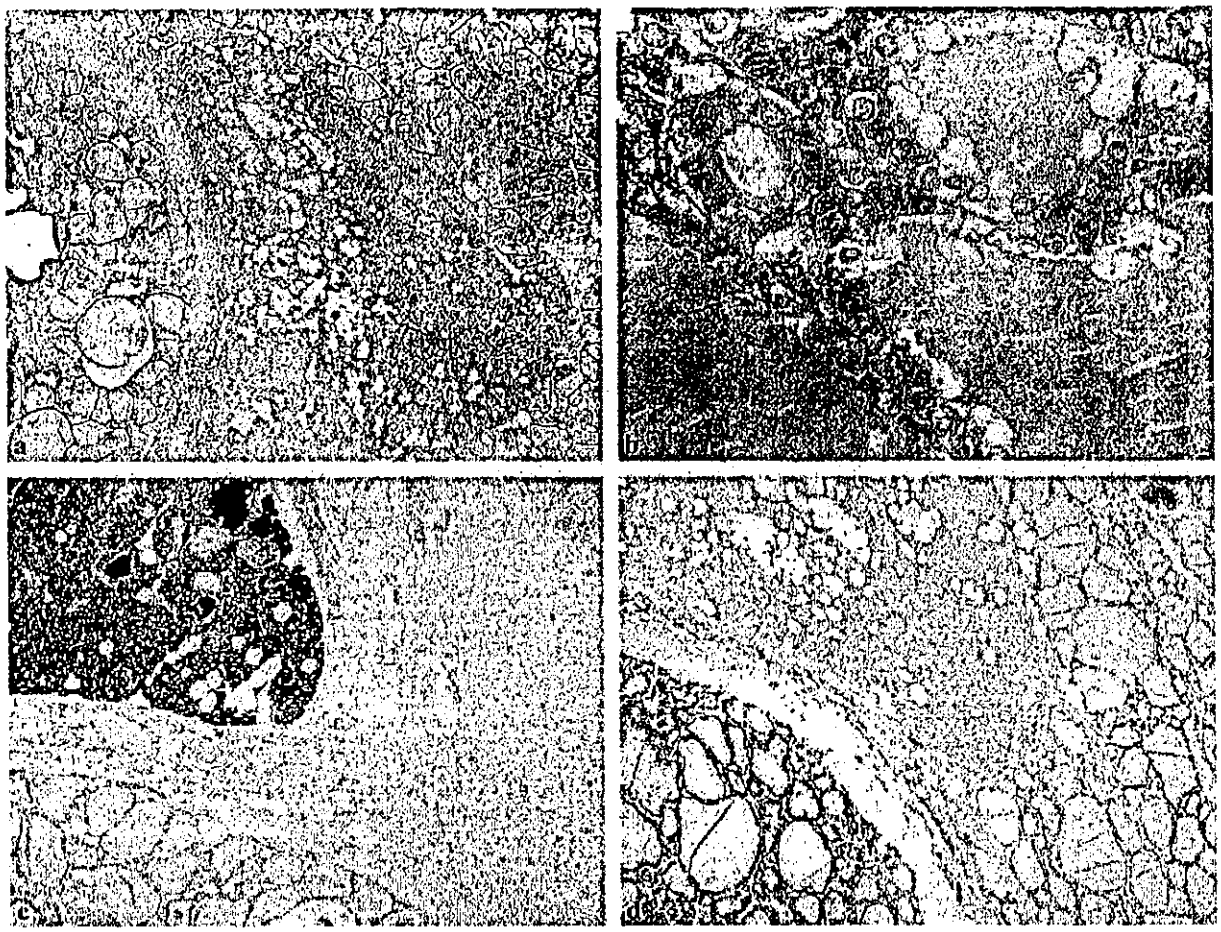

Figure 1. a, The encapsulated papillary microcarcinoma is shown on the left, the ectopic parathyroid gland in the middle, and normal thyroid tissue on the right. Note, the position of the parathyroid gland is in the immediate vicinity of the tumour capsule. b, At higher magnification, the carcinoma shows the typical nuclear features of a papillary tumour with crowding and a ground-glass appearance while the microarchitecture is completely follicular (= 'follicular variant of papillary carcinoma of the thyroid'). c, Immunostaining with an antibody to synaptophysin exhibits strong cytoplasmic staining of the cells of the parathyroid gland clearly demonstrating the endocrine nature of the cells. d, Immunostaining with an antibody to S100 protein decorates the neoplastic cells of the papillary carcinoma while the ectopic parathyroid gland and normal thyroid tissue contain only few scattered recticulum cells. The epithelial cells are not stained.

Expression of HER-2/*neu* gene and protein in salivary duct carcinomas of parotid gland as revealed by fluorescence *in-situ* hybridization and immunohistochemistry

Sir: We have read with interest the article entitled: 'Expression of HER-2/*neu* gene and protein in salivary duct carcinomas of parotid gland as revealed by fluorescence *in-situ* hybridization (FISH) and immuno histochemistry' by Skalova *et al.*[1] This work represents the first molecular assessment by FISH of *HER2* gene status in this rare and aggressive neoplasm showing a histological resemblance to ductal carcinoma of the breast. The authors studied 10 cases by immunocytochemistry and FISH. They found strong immunohistochemical positivity (3+ score) in seven cases, four of which carried *HER2* gene amplification (57%), while three were non-amplified (43%). In three cases the analysis was inconclusive.

We studied *HER2* gene status in formalin-fixed paraffin-embedded tissue sections of 18 consecutive cases of salivary duct carcinoma collected in our institution, according to previous published methodologies.[2] Eleven cases showed a score 3+, eight of which carried *HER2* gene amplification (73%), while three were non-amplified (27%). None of the immunohistochemically negative cases showed amplification.

In comparison with unselected breast carcinoma series, both the investigations outline a higher percentage of both HER-2 3+/amplified cases (25% versus

57–73%)[3] and HER2 3+/non-amplified (i.e. false-positive) cases (3% versus 27–43%)[3] in salivary duct carcinoma.

As far as the pattern of amplification is concerned, Skalova *et al.* described a homogeneously staining region (HSR) pattern in all amplified cases, while we observed three different patterns of amplification: (i) five cases presented amplified genes arranged as HSR, usually one or two per nucleus; (ii) one case showed multiple scattered single-copy HER2 signals and chromosome 17 polisomy (calculated ratio between HER2 and centromeric probe (CEP) 17 copy number was more than 2 in all tumour nuclei); (iii) two cases showed a pattern of hybridization consistent with double minutes (Figure 1), a very unusual occurrence in breast cancer.[4]

Considering the breast model where the efficiency of herceptin-based therapy is restricted to HER2 3+ or amplified cases[5] and assuming that in salivary duct carcinoma the biological basis of response to herceptin is the same as in breast cancer, we can anticipate successful use of this drug in salivary duct carcinoma. On the basis of the above-reported findings it might be expected that >50% of such patients could benefit from TKR-inhibitor therapy. However, the high rate of HER2 3+ non-amplified cases (>27%), likely to be unresponsive, necessitates FISH analysis for patient selection. Assessment by FISH is further supported by our preliminary data regarding the relationship between protein expression and the amplification pattern. Despite the presence of a 3+ immunohistochemical score, we found no HER2 protein by immunoprecipitation and Western blotting experiments in the two cases carrying double minute-related amplification. If this finding is confirmed by further experiments and since the lack of HER2 protein expression is correlated with an unsuccessful response to herceptin therapy, FISH is likely to become the assessment of choice in this salivary tumour type.

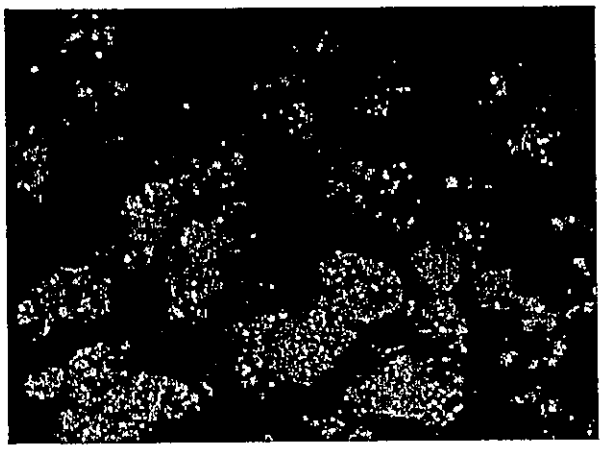

Figure 1. Example of *HER2* gene amplification in salivary duct carcinoma (HER2 signals in orange, centromeric probe (CEP) 17 signals in green). Note the pattern of amplification consistent with the presence of double minutes showing multiple clusters of amplified genes scattered over the nucleus.

ACKNOWLEDGEMENT

This work was supported by 'AIRC 2001 (Associazione Italiana per la Ricerca sul Cancro)', grant no. 420.198.122.

G P Dagrada
T Negri
E Tamborini
M A Pierotti[1,2]
S Pilotti[2]

Experimental Molecular Pathology, Department of Pathology and
[1]*Experimental Oncology Department, Istituto Nazionale per lo Studio e la Cura dei Tumori, Milano, Italy*
[2]*Senior Co-authors*

1. Skalova A, Starek I, Vanecek T *et al.* Expression of HER-2/*neu* gene and protein in salivary duct carcinomas of parotid gland as revealed by fluorescence *in-situ* hybridization and immunohistochemistry. *Histopathology* 2003; 42; 348–356.
2. Dagrada GP, Mezzelani A, Alasio L *et al.* HER-2/neu assessment in primary chemotherapy treated breast carcinoma: no evidence of gene profile changing. *Breast Cancer Res. Treat.* 2003; 80; 207–214.
3. Pauletti G, Godolphin W, Press MF *et al.* Detection and quantitation of HER-2/neu gene amplification in human breast cancer archival material using fluorescence *in situ* hybridization. *Oncogene* 1996; 13; 63–72.
4. Mitelman F. *Catalog of chromosome aberrations in cancer*, 5th ed. New York: Wiley-Liss, 1994.
5. Vogel CL, Cobleigh MA, Tripathy D *et al.* Efficacy and safety of trastuzumab as a single agent in first-line treatment of HER2-overexpressing metastatic breast cancer. *J. Clin. Oncol.* 2002; 20; 719–726.

Malignant mixed epithelial and stromal tumours of the kidney: a report of the first two cases with a fatal clinical outcome

Sir: Mixed epithelial and stromal tumour of the kidney (MESTK), a rare benign neoplasm of unknown aetiology, is a recently established entity unifying several neoplasms such as adult mesoblastic nephroma, cystic hamartoma of the pelvis, adult type cystic nephroma,

multilocular renal cysts, and solid and cystic biphasic tumour of the kidney.[1–4] In cases reported as MESTK, recurrence or fatal outcome has, to date, never been reported. Here, we present two cases of malignant MESTK with local recurrences and fatal outcomes.

The first case was in a 43-year-old Japanese woman, who had undergone radical nephrectomy for a right renal tumour and developed a local recurrent tumour 2 years later. Nine months after extirpation of the recurrent tumour she developed another local recurrence, associated with severe haemorrhage which could not be sufficiently controlled even by three trials of transarterial embolization. The recurrent tumour was found to have invaded adjacent organs allowing only palliative surgery for mass reduction. The patient died 43 months after initial nephrectomy. The second case was in a 31-year-old Japanese woman who had undergone radical nephrectomy for a tumour in the upper pole of the left kidney. Four months after the operation, she developed a local recurrent tumour, accompanied by massive ascites. She died 11 months after nephrectomy.

In case 1, the primary tumour measured approximately 70 mm in diameter, was located mainly near the renal hilus and appeared to consist chiefly of solid components. In case 2 it measured 70 × 70 × 60 mm, was generally well circumscribed and extended beyond the renal capsule. It consisted of solid and cystic components; the former was yellowish and firm and the latter was filled with haematoma.

The primary tumours of both patients were composed of proliferating spindle-shaped cells and epithelial tubular structures of various sizes (Figure 1a). The epithelial components were intermingled with the stromal components throughout the tumours. In case 1, the spindle cells had bright eosinophilic cytoplasm and fusiform nuclei with moderate atypia, formed interlacing bundles and small fascicles with high cellularity (Figure 1b) and infiltrated the renal hilar fat extensively. In case 2, the stromal components were composed of varying numbers of atypical spindle cells with clear cytoplasm that formed fascicles or whorled around the small tubules. No blastema was present. In both cases, the sizes of the epithelial tubular structures were variable, from small tubules reminiscent of normal collecting ducts to cystically dilated ducts lined by cells with a hobnail appearance (Figure 2). All the cells of the epithelial components lacked cytological atypia. It is noteworthy that tubular structures could be seen even in the extrarenally invading part of case 2's tumour and in the recurrent tumour of case 1, confirming that the tubules were not normal structures that had become involved but were integral neoplastic components of the tumours. Mitoses were conspicuous in both cases.

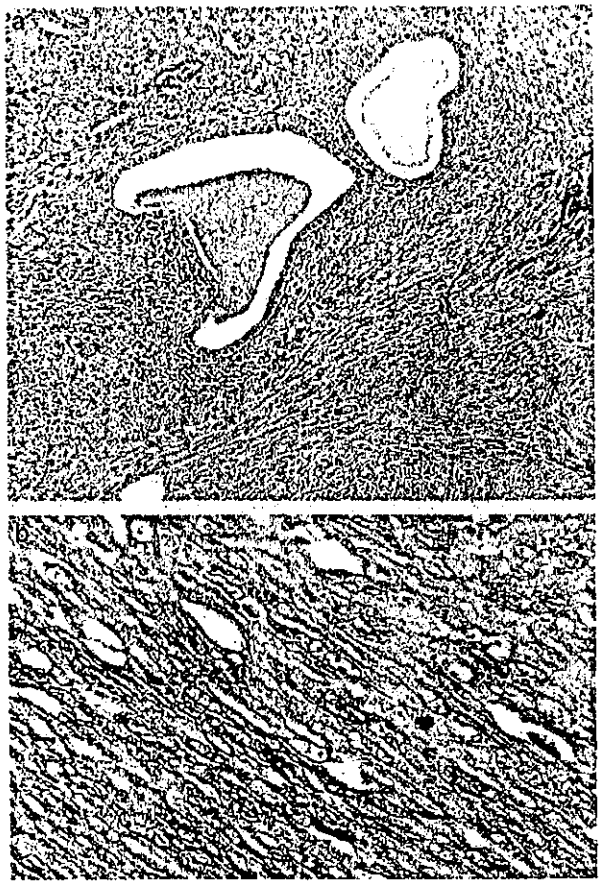

Figure 1. The primary tumour of case 1. a, The tumour is composed mainly of proliferating spindle-shaped cells and epithelial tubular or cystic structures scattered amidst the spindle cells. b, The spindle cells have eosinophilic cytoplasm and fusiform nuclei with moderate atypia and have formed small fascicles with high cellularity. Haematoxylin and eosin.

Immunohistochemically, the spindle cells of both cases were vimentin-positive, and those of case 1 were muscle-specific actin- and α-smooth muscle actin-positive. The cells of the epithelial structures of both cases were cytokeratin- and vimentin-positive and focally epithelial membrane antigen-positive.

The overall histopathological and immunohistochemical findings of these two cases were similar to those of MESTK,[2] but they consisted of more atypical spindle cells forming interlacing fascicles, bundles and whorling around the tubules with increased numbers of mitotic figures.

The differential diagnoses include leiomyosarcoma, biphasic synovial sarcoma[4] and related tumours. Although leiomyosarcoma is the most common mesenchymal tumour arising in the kidney, it contains neither neoplastic epithelial components nor entrapped tubules, because its growth is expansive rather than

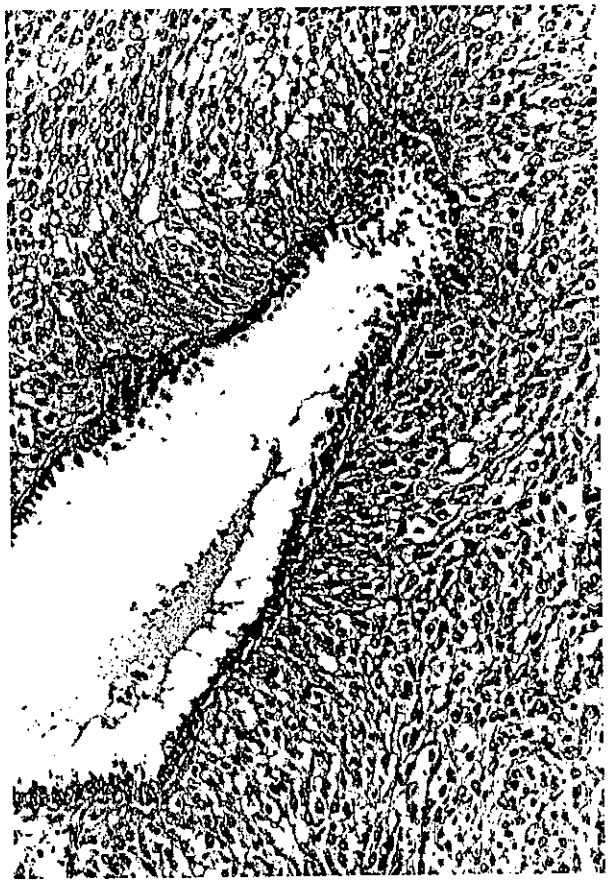

Figure 2. The primary tumour of case 2. Some cystic structures are lined by cells with a hobnail appearance. Haematoxylin and eosin.

infiltrative. Biphasic synovial sarcoma of the kidney is a rare neoplasm that contains both epithelial and stromal components.[5] Even if typical biphasic synovial sarcomas occur in the kidney, their epithelial cells are usually cuboidal or polygonal and form solid nests and glandular or tubular structures,[6] whereas the epithelial components in the present two tumours lacked obvious cytological atypia and were considered to be similar to those of the normal collecting ducts.

In conclusion, rarely, MESTK has a malignant histopathological appearance and behaves aggressively. In this situation, this tumour needs to be distinguished from leiomyosarcoma and synovial sarcoma arising in the kidney.

ACKNOWLEDGEMENTS

This study was supported by a Grant-in-Aid for the Second Term Comprehensive 10-Year Strategy for Cancer Control and a Grant-in-Aid for Cancer Research from the Ministry of Health, Labour and Welfare of Japan.

T Nakagawa
Y Kanai[2]
H Fujimoto
H Kitamura
H Furukawa[1]
S Maeda[3]
T Oyama[4]
T Takesaki[5]
T Hasegawa[2]

Urology and [1]Diagnostic Radiology Divisions, National Cancer Centre Hospital, [2]Pathology Division, National Cancer Centre Research Institute and [3]Department of Pathology, Nippon Medical School Hospital, Tokyo, and [4]Urology and [5]Pathology Divisions, Yamanashi Prefectural Central Hospital, Yamanashi, Japan

1. Michal M, Syrucek M. Benign mixed epithelial and stromal tumor of the kidney. *Pathol. Res. Pract.* 1998; 194; 445–448.
2. Adsay NV, Eble JN, Srigley JR, Jones EC, Grignon DJ. Mixed epithelial and stromal tumor of the kidney. *Am. J. Surg. Pathol.* 2000; 24; 958–970.
3. Michal M. Benign mixed epithelial and stromal tumor of the kidney. *Pathol. Res. Pract.* 2000; 196; 275–276.
4. Svec A, Hes O, Michal M, Zachoval R. Malignant mixed epithelial and stromal tumor of the kidney. *Virchows Arch.* 2001; 439; 700–702.
5. Argani P, Faria PA, Epstein JI *et al.* Primary renal synovial sarcoma: molecular and morphologic delineation of an entity previously included among embryonal sarcomas of the kidney. *Am. J. Surg. Pathol.* 2000; 24; 1087–1096.
6. Tumors of uncertain differentiation and those in which differentiation is nonmesenchymal. In Kempson RL, Fletcher CDM, Evans HL, Hendrickson MR, Sibley RK eds. *Tumors of the soft tissues (Atlas of tumor pathology, Third Series, Fascicle 30)*. Washington, DC: Armed Forces Institute of Pathology, 2001; 419–501.

Neuroendocrine carcinoma of the vulva with paraganglioma-like features

Sir: Neuroendocrine tumours (NTs) of the female genital tract are relatively uncommon.[1] Particularly, NTs occurring in the vulva are extremely rare with the few cases reported in the English literature considered as Merkel cell carcinoma (MCC).[2] Here we document a neuroendocrine vulvar carcinoma with peculiar microscopic, immunohistochemical and ultrastructural features reminiscent of a paraganglioma.

A 62-year-old woman presented with a 20-mm soft, painful lump located in the right upper portion of the labia majora. Abdominothoracic computed tomography (CT) scan excluded the possibility of it being a metastasis from a primary tumour elsewhere. An excisional biopsy was performed and a diagnosis of neuroendocrine carcinoma made. Three months later the neoplasm recurred locally and right inguinal lymphadenopathy was noted. Treatment consisted of radical vulvectomy followed by local radiotherapy. Eight months later a total body CT scan revealed an enlargement of the abdominal and mediastinal lymph nodes. Nineteen months after the original diagnosis the patient is still alive with multiple abdominal and thoracic metastases.

Histologically, the tumour involved the dermis and subcutis and showed a prevalent organoid or 'Zellballen' pattern of growth (Figure 1a). Occasionally, hypercromatic, slender cells, resembling sustentacular cells, outlined the neoplastic nests.

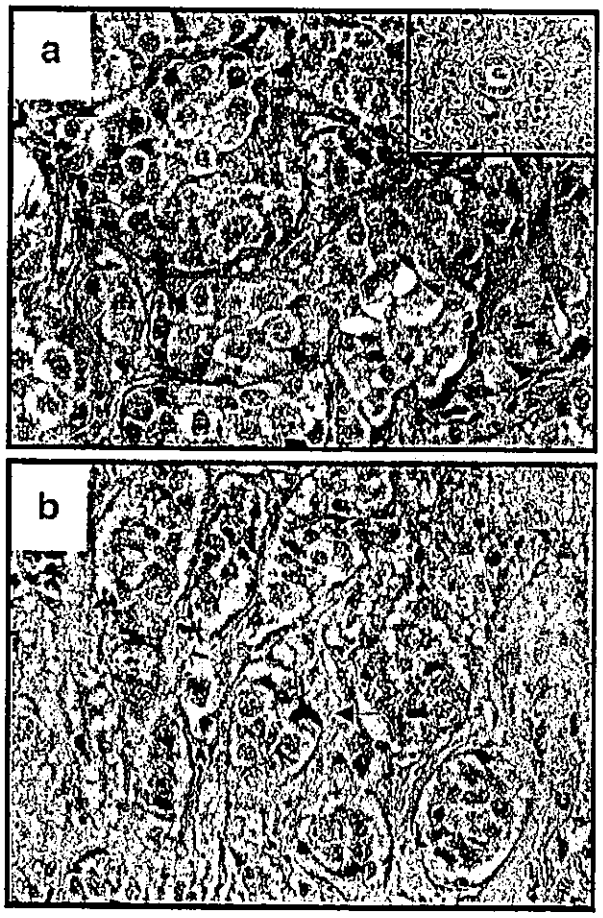

Figure 1. a Neoplastic cells were mainly disposed in organoid nests. Inset: rare glandular structures were found in another microscopic field. b, Immunohistochemically, S100 protein outlined a residual stellate/dendritic cell at the periphery of a tumour nest (arrow).

Tumour cells were medium in size, with abundant clear to eosinophilic cytoplasm; nuclei were round to oval with fine chromatin and occasional nucleoli. Mitotic figures, apoptotic bodies, foci of tumour necrosis, vascular invasion, and occasional glandular or pseudoglandular structures (Figure 1a, inset) were observed. Metastatic nodal disease was morphologically similar to the primary vulvar neoplasm.

Neoplastic cells were immunoreactive for cytokeratin 8 and 18, carcinoembryonic antigen (CEA), synaptophysin, PGP9.5 and neuron-specific enolase but were negative for cytokeratin 20, chromogranin A, and TTF-1. Protein S100 decorated occasional cells at the periphery of the 'Zellballen' (Figure 1b).

Electron microscopy was performed from a paraffin block. Tumour cells contained numerous dispersed cytoplasmic membrane-bound dense granules and exhibited features of epithelial differentiation including cell junctions. Moreover, electron microscopy showed the presence of long, slender sustentacular cells, outlining the epithelial nests.

On the basis of the morphological, immunohistochemical, ultrastructural and clinical findings a final diagnosis of neuroendocrine carcinoma of the vulva with paraganglioma-like features was made. The differential diagnosis included metastatic neuroendocrine carcinoma, malignant paraganglioma and MCC. Careful clinical evaluation and the absence of a previous history of a neuroendocrine neoplasm help to rule out a metastasis.

The 'Zellballen' growth pattern and the presence of sustentacular cells suggested a diagnosis of paraganglioma. A case of paraganglioma without malignant features occurring in the vulva has been reported.[3] However, in the present case the presence of glands, the strong cytokeratin and CEA immunoreactivity, and the ultrastructurally evident desmosomal junctions strongly supported an epithelial origin of the lesion. Paraganglioma stains for neuroendocrine markers, but is not usually reactive for cytokeratin and CEA. Although occasional examples of paraganglioma have been reported to be immumoreactive for keratin,[4] CEA immunostaining has never been described in this tumour.[5] Moreover, it is noteworthy that the presence of sustentacular cells is not exclusive to paragangliomas.[6]

Although the few reports describing primary neuroendocrine carcinoma of the vulva support its origin from epidermal Merkel cells, this case did not show the typical immunohistochemical and ultrastructural features of MCC.[2]

The origin of primary vulvar neuroendocrine carcinomas is particularly intriguing.[7,8] In the present case the apparent lack of any relationship with vestibular glands and the absence of morphological features other than neuroendocrine strongly support an origin from solitary or aggregated cells of the diffuse/dispersed neuroendocrine system.

Whether the present case is simply a histological curiosity or has clinical significance is a moot point. We suggest that the diagnosis of neuroendocrine carcinoma, even with an unusual morphological appearance, should always be taken into account, since these tumours have a highly malignant clinical course, with disseminated disease usually occurring within 1 year following diagnosis.

P G Nuciforo
F Fraggetta[1]
R Fasani
P Braidotti
G Nuciforo[2]

Department of Medicine, Surgery and Dental Sciences, University of Milan, A. O. S. Paolo and IRCCS Ospedale Maggiore, Milan, [1]Department of Pathology, Ospedale Cannizzaro, Catania, and [2]Department of Pathology, A.O. Vittorio Emanuele-S. Bambino, Catania, Italy

1. Eichhorn JH, Young RH. Neuroendocrine tumors of the genital tract. *Am. J. Clin. Pathol.* 2001; 115; S94–S112.
2. Hierro I, Blanes A, Matilla A, Munoz S, Vicioso L, Nogales FF. Merkel cell (neuroendocrine) carcinoma of the vulva. A case report with immunohistochemical and ultrastructural findings and review of the literature. *Pathol. Res. Pract.* 2000; 196; 503–509.
3. Colgan TJ, Dardick I, O'Connell G. Paraganglioma of the vulva. *Int. J. Gynecol. Pathol.* 1991; 10; 203–208.
4. Chetty R, Pillay P, Jaichand V. Cytokeratin expression in adrenal phaeochromocytomas and extra-adrenal paragangliomas. *J. Clin. Pathol.* 1998; 51; 477–478.
5. LaGuette J, Matias-Guiu X, Rosai J. Thyroid paraganglioma: a clinicopathologic and immunohistochemical study of three cases. *Am. J. Surg. Pathol.* 1997; 21; 748–753.
6. Al-Khafaji B, Noffsinger AE, Miller MA *et al.* Immunohistologic analysis of gastrointestinal and pulmonary carcinoid tumors. *Hum. Pathol.* 1998; 29; 992–999.
7. Pearse AGE, Takor TT. Embriology of the diffuse neuroendocrine system and its relationship to the common peptides. *Fed. Proc.* 1979; 32; 2288–2294.
8. Slone S, Reynolds L, Gali S *et al.* Localization of chromogranin, synaptophysin, serotonin, and CXCR2 in neuroendocrine cells of the minor vestibular glands: an immunohistochemical study. *Int. J. Gynecol. Pathol.* 1999; 18; 360–365.